JACS
JOURNAL OF THE AMERICAN CHEMICAL SOCIETY
Communication
pubs.acs.org/JACS

# Deciphering the Spatial Arrangement of Metals and Correlation to Reactivity in Multivariate Metal–Organic Frameworks

Qi Liu,[†] Hengjiang Cong,[†] and Hexiang Deng*[,†,§]

[†]Key Laboratory of Biomedical Polymers-Ministry of Education, College of Chemistry and Molecular Sciences and [§]The Institute for Advanced Studies, Wuhan University, Wuhan 430072, China

Supporting Information

**ABSTRACT:** Thirty-six porphyrin-based metal–organic frameworks (MOFs) with composition of $(M_3O)_2$(TCPP-M)$_3$ and $M_3O$ trigonal SBUs of various metals, $Mg_3O$, $Mn_3O$, $Co_3O$, $Ni_3O$, and $Fe_3O$ including mixed-metal SBUs, $Mn_xFe_{3-x}O$, $Ni_xFe_{3-x}O$, $Co_xNi_{3-x}O$, $Mn_xCo_{3-x}O$, $Mn_xMg_{3-x}O$, and $Mn_xNi_{3-x}O$ were synthesized and characterized. These multivariate MOFs (MTV-MOFs) were examined by X-ray photoelectron spectroscopy, UV–vis diffuse reflectance spectra, and for the first time, their metal spatial arrangement deciphered and were found to exist in the form of either domains or well-mixed. We find that MTV-MOFs with well-mixed metals in their SBUs, rather than the SBUs having one kind of metal but different from one SBU to another, perform better than the sum of their parts in the test reaction involving the photo-oxidation of 1,5-dihydroxynaphthalene.

Multivariate metal–organic frameworks (MTV-MOFs), in which organic linkers have multiple functional groups, have been found to function in a manner where the whole performs better than the sum of the parts.[1] The analogous chemistry involving the incorporation of multiple metals in a MOF structure is also being developed because mixing of metals is widely recognized as an essential feature to achieving optimal catalytic, optical, and electronic properties or even mimicking protein catalytic centers containing multiple metals.[2] In general, both MTV-MOF systems suffer from the fact that the various organic functionalities lie on the same crystallographic position, and similarly for the case of metal ions. Thus, X-ray diffraction (XRD) techniques offer limited information in deciphering the spatial arrangement of these components.[3] Here, we identified a MOF with a structure ideally suited for incorporating multivariate metal ions in both the organic linkers as well as the metal oxide secondary building units (SBUs) (Figure 1). The organic linker is tetrakis (4-carboxyphenyl) porphyrin (TCPP) without (TCPP-$H_2$) and with metals in the porphyrin unit of the linker, TCPP-Mg, TCPP-Co, TCPP-Ni, TCPP-Cu, and TCPP-Zn. These were linked to $M_3O$ trigonal SBUs of various metals, $Mg_3O$, $Mn_3O$, $Co_3O$, $Ni_3O$, and $Fe_3O$ including MTV metal SBUs, $Mn_xFe_{3-x}O$, $Ni_xFe_{3-x}O$, $Co_xNi_{3-x}O$, $Mn_xNi_{3-x}O$, and $Mn_xMg_{3-x}O$ to give the corresponding series of 36 MOFs with the general composition of $(M_3O)_2$(TCPP-M)$_3$ (water molecules in SBU were deleted for clarity) (Figure 1). We show that for the series of $(M_3O)_2$(TCPP-M)$_3$ in which each of the SBU and the TCPP have one kind of metal, the composition

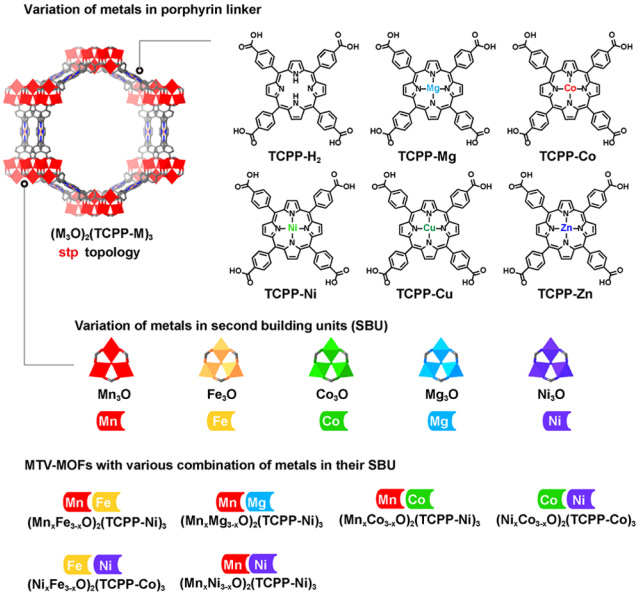


**Figure 1.** Single component MOF series, $(M_3O)_2$(TCPP-M)$_3$, constructed by five different SBUs and six different porphyrin linkers, and corresponding MTV-MOFs with mixed-metal SBUs.

$(Mn_3O)_2$(TCPP-Ni)$_3$ has the highest conversion rate ($k_{obs}$ = 81.5 × $10^{-2}$ $h^{-1}$) for the photo-oxidation of 1,5-dihydroxynaphthalene as a test reaction.[4] We also show that among the MTV-MOF series (mixed metals in the SBU), the composition $(Mn_{1.77}Ni_{1.23}O)_2$(TCPP-Ni)$_3$ exhibits further enhancement in reactivity ($k_{obs}$ = 1.03 $h^{-1}$) toward the same reaction. More importantly, we have used spectroscopic techniques (XPS and UV–vis diffuse reflectance spectra (DRS)) to successfully decipher, for the first time, the spatial arrangement of metal ions in the MTV-MOF systems to distinguish two scenarios of mixing metals within and between SBUs. The impact of these two distinct mixed metal scenarios on the band gap of the MOF and the correlation to the reactivity of the system are also outlined.

Single component MOFs, $(M_3O)_2$(TCPP-M)$_3$, are synthesized through mixing the corresponding metal source with one of the organic linkers, $H_4$TCPP-M, acetic acid, and trifluoroacetic acid in DMF, and heating the mixture at 150 °C in glass vials for 12 to 36 h [Section S3, Supporting Information (SI)]. Various

**Received:** August 24, 2016
**Published:** October 5, 2016




DOI: 10.1021/jacs.6b08724
J. Am. Chem. Soc. 2016, 138, 13822–13825

combinations of SBUs and organic linkers generated 27 different single component MOFs, all with rod shaped crystals large enough for single crystal X-ray analysis. Results show that these MOFs are isoreticular with hexagonal topology (**stp**) and all crystallized into an identical space group of *P6/mmm* (Figures 1 and S1).[5] Each of the SBU has the general formula $M_3O(COO)_6(H_2O)_3$, abbreviated as $M_3O$ (M = Mg, Mn, Fe, Co, Ni) to avoid the complexity in oxidation state of SBU-metals in the following text.[6] In order to balance the charge in the formula, counteranion/cation were added based on the elemental analysis results (Section S3, SI). The powder X-ray diffraction (PXRD) patterns of the as-synthesized samples of these MOFs match well with the pattern simulated from single crystal structure data, indicating phase purity of the bulk samples (Figures S2−S6). The maintenance of the crystallinity of these activated MOFs is evidenced by the sharp peaks in their PXRD patterns (Figures S21−S24).

MTV-MOFs composed of multiple metals are synthesized and activated under similar conditions as the single component MOFs but with mixed metal sources added to the reaction. The metal content of the resulting MTV-MOFs can be controlled through varying the stoichiometry of the starting materials (SI). Single crystal XRD analysis of the MTV-MOFs shows that they have the same structure as the single component MOFs (Figure 1 and SI). PXRD patterns of the bulk samples also confirm the phase purity of these MTV-MOFs (Figures S7−S12). The compositions of MTV-MOFs were quantified to be derived as $[(\mathbf{M1})_{3-x}(\mathbf{M2})_xO]_2(\mathbf{TCPP\text{-}M})_3$. The detailed composition of each MTV-MOF is listed in the Tables S1−S3.

The permanent porosity of the guest-free MOFs is confirmed by the $N_2$ adsorption measurements at 77K (Figures S34−S41). The calculated Brunauer−Emmett−Teller (BET) surface areas of selected single component MOFs, $(\mathbf{Ni_3O})_2(\mathbf{TCPP\text{-}Cu})_3$, $(\mathbf{Ni_3O})_2(\mathbf{TCPP\text{-}Co})_3$, $(\mathbf{Fe_3O})_2(\mathbf{TCPP\text{-}Co})_3$, and MTV-MOF, $(\mathbf{Mn_{1.77}Ni_{1.23}O})_2(\mathbf{TCPP\text{-}Ni})_3$, are 2200, 2090, 1660, and 1380 $m^2\ g^{-1}$, respectively. The $N_2$ isotherms of these MOFs are type IV, which is typical for mesoporous materials, and the starting point of the second step is observed at $P/P_0 = 0.20$, corresponding to a pore size of 3.2 nm, in good agreement with their single crystal structure (Figures S1, S14, and S15). Several MOFs exhibit limited $N_2$ adsorption upon guest removal, however, their SBU-linker connections were conserved. Synchrotron X-ray absorption analysis of these MOFs reveals that the coordination environment of metals was maintained as reflected in the good fit between the experimental data and the profile simulated from the single crystal structure of the MOFs (Figures S58−S70).[7]

Although several MTV-MOF systems with multivariate metals have been reported, the specific arrangement of metals throughout the crystal structure remains unknown.[8] It is difficult because XRD analysis provides limited distinction between metal atoms of similar sizes. This becomes even more challenging when their crystallographic position is the same. There are two scenarios for the spatial arrangements of metals in a MTV-MOF composed of two SBU metals: (1) the domain arrangement, where two different SBUs, each of which is composed of three metal atoms of the same kind, are mixed to form domains in the MOF structure (Figure 2A), and (2) the well-mixed arrangement, where there are two kind of metals in the same SBU and these mixed metal SBUs are present throughout the entire MOF crystal (Figure 2B).

Prior to deciphering these two scenarios for metal arrangements in MTV-MOFs, we need to make sure that the MTV-

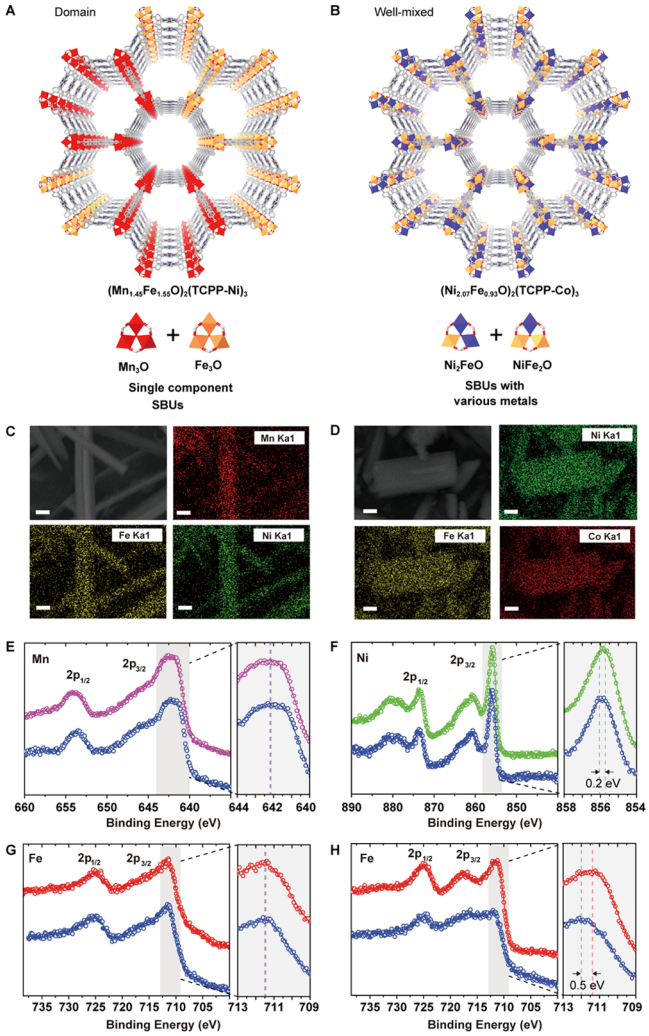


**Figure 2.** (A, B) Two spatial arrangements in mixed-metal MTV-MOFs and their SBUs. (C, D) SEM images and EDX mappings of $(\mathbf{Mn_{1.45}Fe_{1.55}O})_2(\mathbf{TCPP\text{-}Ni})_3$ and $(\mathbf{Ni_{2.07}Fe_{0.93}O})_2(\mathbf{TCPP\text{-}Co})_3$, respectively (scale bar, 2 $\mu$m). (E, G) XPS overlay of MTV-MOF, $(\mathbf{Mn_{1.45}Fe_{1.55}O})_2(\mathbf{TCPP\text{-}Ni})_3$ (blue line) with the its single component counterparts, $(\mathbf{Mn_3O})_2(\mathbf{TCPP\text{-}Ni})_3$ (magenta line) and $(\mathbf{Fe_3O})_2(\mathbf{TCPP\text{-}Ni})_3$ (red line). (F, H) XPS overlay of MTV-MOF, $(\mathbf{Ni_{2.07}Fe_{0.93}O})_2(\mathbf{TCPP\text{-}Co})_3$ (blue line), with the its single component counterparts, $(\mathbf{Ni_3O})_2(\mathbf{TCPP\text{-}Co})_3$ (green line) and $(\mathbf{Fe_3O})_2(\mathbf{TCPP\text{-}Co})_3$ (red line).

MOF is not a heterogeneous physical mixture of MOF crystals of different metals. In order to rule out this possibility, we applied energy dispersive spectra (EDS) to map the presence of various metals using scanning electron microscopy (SEM). Two MTV-MOFs, $(\mathbf{Mn_{1.45}Fe_{1.55}O})_2(\mathbf{TCPP\text{-}Ni})_3$ and $(\mathbf{Ni_{2.07}Fe_{0.93}O})_2(\mathbf{TCPP\text{-}Co})_3$, are used here as illustrative examples. For the first MTV-MOF, if it was a physical mixture of $(\mathbf{Mn_3O})_2(\mathbf{TCPP\text{-}Ni})_3$ and $(\mathbf{Fe_3O})_2(\mathbf{TCPP\text{-}Ni})_3$, we would expect to observe the presence of Mn and Fe separately in their corresponding crystal specimens. However, the EDS mapping shows that both Mn and Fe are distributed homogeneously within all crystals of the sample (Figure 2C). This clearly indicates that this MTV-MOF is not a physical mixture. Similar observations were made for samples of $(\mathbf{Ni_{2.07}Fe_{0.93}O})_2(\mathbf{TCPP\text{-}Co})_3$ (Figure 2D).

However, due to the resolution limit of EDS in SEM,[9] EDS mapping is not sufficiently accurate to differentiate the two


DOI: 10.1021/jacs.6b08724
J. Am. Chem. Soc. 2016, 138, 13822−13825

scenarios of MTV-MOFs at the atomic scale. Thus, we turned to XPS to study the coordination environment of the metals in the SBUs. If there are two kinds of metals in the same SBU, the coordination environments of the metals of each kind will be influenced by the presence of adjacent ones of different kinds. These changes can be detected by XPS. In the domain scenario, the interaction between two kinds of metals is negligible because they are separated by the linkers. XPS data for $(\mathbf{Mn_{1.45}Fe_{1.55}O})_2(\mathbf{TCPP\text{-}Ni})_3$ give almost identical binding energies for $Mn^{2+}$ and $Fe^{3+}$ as their single component counterparts, $(\mathbf{Mn_3O})_2(\mathbf{TCPP\text{-}Ni})_3$ and $(\mathbf{Fe_3O})_2(\mathbf{TCPP\text{-}Ni})_3$, respectively (Figure 2E,G). Thus, the Mn and Fe metals are in separate SBUs for $(\mathbf{Mn_{1.45}Fe_{1.55}O})_2(\mathbf{TCPP\text{-}Ni})_3$, and the spatial arrangements of metals follow the domain scenario. In contrast, significant shifts in binding energy are observed in the case of $(\mathbf{Ni_{2.07}Fe_{0.93}O})_2(\mathbf{TCPP\text{-}Co})_3$ in comparison to the single component MOFs, $(\mathbf{Ni_3O})_2(\mathbf{TCPP\text{-}Co})_3$ and $(\mathbf{Fe_3O})_2(\mathbf{TCPP\text{-}Co})_3$ (Figure 2F,H). The Ni $2p_{2/3}$ peak shifted by 0.2 eV and the Fe $2p_{2/3}$ peak shifted by 0.5 eV, respectively. These results prove that the Fe and Ni metals are in the same SBUs for the MTV-MOF $(\mathbf{Ni_{2.07}Fe_{0.93}O})_2(\mathbf{TCPP\text{-}Co})_3$, adopting the well-mixed scenario. In order to rule out the influence from oxidation states on the determination of metal spatial arrangement, a combination of spectroscopic techniques were applied including XANES, Mössbauer and EPR (SI). The results clearly confirm that each of the metals in the SBU has only one single oxidation state in both well-mixed and domain spatial arrangements. Specifically, Mn, Co, Ni, and Fe exhibit the oxidation state of +2, +2, +2, and +3, respectively. The existence of two scenarios of metal arrangement in MTV-MOFs may originate from differences in the ionic radius of the metals and their affinity to coordinate with oxygen.[10] Given the ionic radius ($Mn^{2+}$ 0.97 Å, $Fe^{3+}$ 0.79 Å, and $Ni^{2+}$ 0.83 Å)[11] and the electronegativity (Mn 1.55, Fe 1.83, Ni 1.91),[12] the similarity between $Ni^{2+}$ and $Fe^{3+}$ allows them to be compatible to present in the same SBU and form the well-mixed arrangement; while the significant difference between $Mn^{2+}$ and $Fe^{3+}$ leads to aggregation to form the domain arrangement.

Noting that the band structure might be altered with the mixing of metals,[2d] we sought to test the catalytic performance of MTV-MOFs having domain or well-mixed metal arrangement. Here, we used a common photocatalytic reaction to test the impact of various band structures of these MTV-MOFs and to correlate their reactivity with the kind and ratio of various metals present in their SBUs. This also provides further comparisons to elucidate the different behavior exhibited by the two spatial arrangements. Photo-oxidation of 1,5-dihydroxynaphthalene (DHN) was used as a model reaction with the MOFs being the catalysts. Upon light absorption, singlet oxygen is generated by the electron excited from the MOFs as illustrated by $(\mathbf{Mn_3O})_2(\mathbf{TCPP\text{-}Ni})_3$ (Figure 3A), then this singlet oxygen reacts with DHN to produce 5-hydroxynaphthalene-1,4-dione (Juglone).[13] By monitoring the concentration of DHN and Juglone in solution using their fingerprint in the UV–vis spectra, the kinetics of this reaction can be revealed (Figure 3B). The effects of metals in the SBU and organic linkers in the photoreaction kinetics were systematically investigated in single component MOFs. Their conversion rates ($k_{obs}$) range from 42.9 to 81.5 × $10^{-2}$ $h^{-1}$ in the order of TCPP-Ni > TCPP-Co > TCPP-Mg > TCPP-Cu > TCPP-$H_2$, keeping the metals in the SBU constant. Similarly, varying the metals in SBU leads to different $k_{obs}$ ranging from 39.5 to 81.5 × $10^{-2}$ $h^{-1}$ in the order of $Mn_3O$ > $Co_3O$ > $Ni_3O$ > $Fe_3O$ > $Mg_3O$, keeping the organic

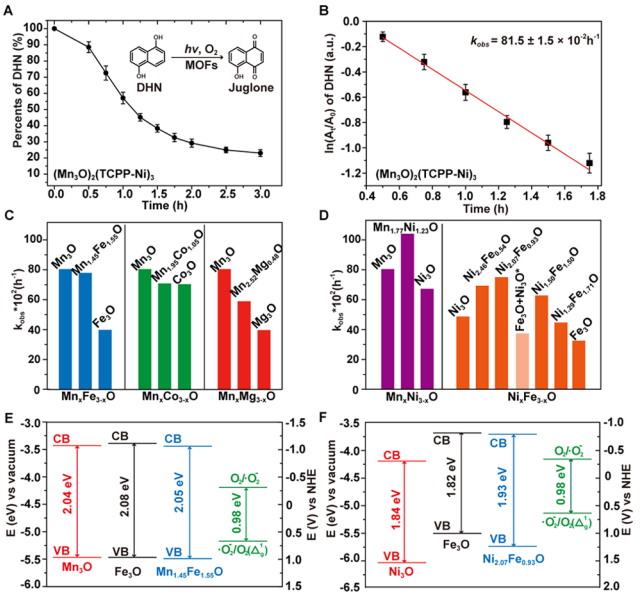


**Figure 3.** (A) Kinetic study of the photocatalytic reaction using $(\mathbf{Mn_3O})_2(\mathbf{TCPP\text{-}Ni})_3$ as a catalyst by monitoring the concentration of DHN molecules in the solution. (Insert) Photo-oxidation of DHN to produce Juglone by oxygen. (B) The conversion rate $k_{obs}$ deduced from $\ln(A_t/A_0)$ versus time. (C) Comparison between $k_{obs}$ of MTV-MOFs in domain metal arrangement and those of their corresponding single component MOFs with porphyrin-Ni. (D) Comparison between $k_{obs}$ of MTV-MOFs in well-mixed metal arrangement with those of their corresponding single component MOFs. (E) Band gap of a MTV-MOF in domain metal arrangement, $(\mathbf{Mn_{1.45}Fe_{1.55}O})_2(\mathbf{TCPP\text{-}Ni})_3$, and its single component MOF counterparts, $(\mathbf{Mn_3O})_2(\mathbf{TCPP\text{-}Ni})_3$ and $(\mathbf{Fe_3O})_2(\mathbf{TCPP\text{-}Ni})_3$. (F) Band gap of a MTV-MOF in well-mixed metal arrangement, $(\mathbf{Ni_{2.07}Fe_{0.93}O})_2(\mathbf{TCPP\text{-}Co})_3$, and its single component MOF counterparts, $(\mathbf{Ni_3O})_2(\mathbf{TCPP\text{-}Co})_3$ and $(\mathbf{Fe_3O})_2(\mathbf{TCPP\text{-}Co})_3$.

linker composition constant. It is worth noting that the catalytic performances of all these MOFs are significantly higher than the discrete unlinked porphyrin linker, TCPP-Co, which only exhibits a $k_{obs}$ of 18.5 × $10^{-2}$ $h^{-1}$. The optimum combination in this MOF series is that in $(\mathbf{Mn_3O})_2(\mathbf{TCPP\text{-}Ni})_3$, with the $k_{obs}$ of 81.5 × $10^{-2}$ $h^{-1}$, which is 330% better than the TCPP linker. Furthermore, synchrotron X-ray absorption spectra (XAS) of MOFs before and after catalysis match closely, indicating the stability of their structure during catalysis (Figures S58–S70).

Next, we examined the photocatalytic performance of MTV-MOFs having the two different spatial arrangements of metals. MTV-MOFs of the domain spatial arrangement composed of $Mn_xFe_{3-x}O$, $Mn_xCo_{3-x}O$ and $Mn_xMg_{3-x}O$ SBUs exhibit catalytic rates falling in between their corresponding MOFs with single component SBU metal (Figure 3C). In the case of MTV-MOFs of the well-mixed spatial arrangement composed of $Mn_xNi_{3-x}O$ and $Ni_xFe_{3-x}O$, their conversion rates exceed the best of their corresponding single component MOFs, and $(\mathbf{Mn_{1.77}Ni_{1.23}O})_2(\mathbf{TCPP\text{-}Ni})_3$ exceeds all the MTV-MOFs with domains (Figure 3D). Specifically, $(\mathbf{Mn_{1.77}Ni_{1.23}O})_2(\mathbf{TCPP\text{-}Ni})_3$ shows a further 26% increase in the catalytic performance ($k_{obs}$ = 1.03 $h^{-1}$) in comparison to its best single component MOF counterpart $(\mathbf{Mn_3O})_2(\mathbf{TCPP\text{-}Ni})_3$. $(\mathbf{Ni_{2.07}Fe_{0.93}O})_2(\mathbf{TCPP\text{-}Co})_3$ shows a conversion rate of $k_{obs}$ = 78.3 × $10^{-2}$ $h^{-1}$, 54% better than its best single component MOF counterpart $(\mathbf{Ni_3O})_2(\mathbf{TCPP\text{-}Co})_3$ ($k_{obs}$ = 50.8 × $10^{-2}$ $h^{-1}$). The control experiment using the physical mixture of 50%


DOI: 10.1021/jacs.6b08724
J. Am. Chem. Soc. 2016, 138, 13822–13825

$(Fe_3O)_2(TCPP\text{-}Co)_3$ and 50% $(Ni_3O)_2(TCPP\text{-}Co)_3$ shows, as expected, a conversion rate between the value of pure $(Fe_3O)_2(TCPP\text{-}Co)_3$ and pure $(Ni_3O)_2(TCPP\text{-}Co)_3$ and significantly lower than well-mixed MTV-MOFs of the same metal component. Indeed, this clearly shows that the well-mixed spatial arrangement within the SBUs leads to better performance than the sum of the parts. The best conversion rate in this MTV-MOF series was found in $(Ni_{2.07}Fe_{0.93}O)_2(TCPP\text{-}Co)_3$ with Ni/Fe ratio close to 2:1, which corresponds to two $Ni^{2+}$ ions and one $Fe^{3+}$ ion in each well-mixed metal SBU.

In order to uncover the reason for the better catalytic performance observed for mixed metal MTV-MOFs, we obtain the band structure of these photocatalysts using UV−vis DRS to determine the absolute band gap in combination with valence band-XPS to reveal the precise position of the valence band (Figures 3E,F and SI). We found that when the SBUs of different metals were aggregated in domains, the corresponding band structure is very close to the single component MOF. On the other hand, when the different metals are present in the same SBU and are well-mixed, their band gaps change dramatically. For example, in the case of $(Ni_{2.07}Fe_{0.93}O)_2(TCPP\text{-}Co)_3$, its band gap shows better overlap with that of the singlet oxygen, which favors electron/hole transfer to oxygen leading to accelerated reaction rate (Figure 3F).[14] Although domain MTV-MOF $(Mn_{1.45}Fe_{1.55}O)_2(TCPP\text{-}Ni)_3$ shows negligible difference with its corresponding single SBU metal MOFs, $(Mn_3O)_2(TCPP\text{-}Ni)_3$ and $(Fe_3O)_2(TCPP\text{-}Ni)_3$, in energy level structures, the differences in their conversion rate can be observed. This is attributed to differences in their light absorption ability (Figures 3E and S79).

In conclusion, we were able to decipher the spatial arrangement in multimetal MTV-MOFs and found that the metals are distributed either in a domain or in well-mixed spatial arrangements. The latter scenario profoundly influences the reactivity of the MOF as evidenced by the reaction rates and as supported by their band gap.

## ■ ASSOCIATED CONTENT

### Supporting Information

The Supporting Information is available free of charge on the ACS Publications website at DOI: 10.1021/jacs.6b08724.

Crystallographic data (ZIP)
Experimental details and data (PDF)

## ■ AUTHOR INFORMATION


### Corresponding Author

*hdeng@whu.edu.cn


### Notes

The authors declare no competing financial interest.

## ■ ACKNOWLEDGMENTS

The XAS and single crystal XRD were performed using beamline BL14W, BL15U, and BL17U1 in Shanghai Synchrotron Radiation (SSRF). EPR were collected at High Magnetic Field Laboratory of the China Academy of Sciences in Hefei (CHMFL). Mössbauer Spectroscopy was measured at Dalian Institute of Chemical Physics, Chinese Academy of Sciences (DICP). We thank Prof. Rui Si (SSRF), Prof. Junhu Wang (DICP), Yufei Shu, Xiaohui Xu, Xuan Gong (Wuhan University) for their invaluable help and discussion. Financial support was provided by the 1000 Talent Plan of China, National Natural Science Foundation of China (21471118, 91545205), and National Key Basic Research Program of China (2014CB239203). Crystallographic data for the reported crystal structures have been deposited at the Cambridge Crystallographic Data Centre via www.ccdc.cam.ac.uk with the codes 1498027−1498032 and 1500181−1500182.

## ■ REFERENCES


(1) (a) Deng, H.; Doonan, C. J.; Furukawa, H.; Ferreira, R. B.; Towne, J.; Knobler, C. B.; Wang, B.; Yaghi, O. M. *Science* **2010**, *327*, 846. (b) Burrows, A. D. *CrystEngComm* **2011**, *13*, 3623. (c) Zhang, Y.-B.; Furukawa, H.; Ko, N.; Nie, W.; Park, H. J.; Okajima, S.; Cordova, K. E.; Deng, H.; Kim, J.; Yaghi, O. M. *J. Am. Chem. Soc.* **2015**, *137*, 2641. (d) Yuan, S.; Lu, W.; Chen, Y. P.; Zhang, Q.; Liu, T. F.; Feng, D.; Zhou, H. C. *J. Am. Chem. Soc.* **2015**, *137*, 3177.

(2) (a) White, K. A.; Chengelis, D. A.; Gogick, K. A.; Stehman, J.; Rosi, N. L.; Petoud, S. *J. Am. Chem. Soc.* **2009**, *131*, 18069. (b) Cui, Y.; Xu, H.; Yue, Y.; Guo, Z.; Yu, J.; Chen, Z.; Gao, J.; Yang, Y.; Qian, G.; Chen, B. *J. Am. Chem. Soc.* **2012**, *134*, 3979. (c) Tu, B.; Pang, Q.; Wu, D.; Song, Y.; Weng, L.; Li, Q. *J. Am. Chem. Soc.* **2014**, *136*, 14465. (d) Brown, K. A.; Harris, D. F.; Wilker, M. B.; Rasmussen, A.; Khadka, N.; Hamby, H.; King, P. W. *Science* **2016**, *352*, 448. (e) Fukushima, T.; Horike, S.; Inubushi, Y.; Nakagawa, K.; Kubota, Y.; Takata, M.; Kitagawa, S. *Angew. Chem., Int. Ed.* **2010**, *49*, 4820. (f) Zheng, S.-T.; Wu, T.; Zuo, F.; Chou, C.; Feng, P.; Bu, X. *J. Am. Chem. Soc.* **2012**, *134*, 1934. (g) Li, P.-Z.; Wang, X.-J.; Liu, J.; Lim, J.-S.; Zou, R.; Zhao, Y. *J. Am. Chem. Soc.* **2016**, *138*, 2142.

(3) (a) Wang, L. J.; Deng, H.; Furukawa, H.; Gándara, F.; Cordova, K. E.; Peri, D.; Yaghi, O. M. *Inorg. Chem.* **2014**, *53*, 5881. (b) Kong, X.; Deng, H.; Yan, F.; Kim, J.; Swisher, J. A.; Smit, B.; Yaghi, O. M.; Reimer, J. A. *Science* **2013**, *341*, 882. (c) Brozek, C. K.; Dincă, M. *J. Am. Chem. Soc.* **2013**, *135*, 12886. (d) Zhai, Q. G.; Bu, X.; Mao, C.; Zhao, X.; Feng, P. *J. Am. Chem. Soc.* **2016**, *138*, 2524.

(4) (a) Schweitzer, C.; Schmidt, R. *Chem. Rev.* **2003**, *103*, 1685. (b) DeRosa, M. C.; Crutchley, R. J. *Coord. Chem. Rev.* **2002**, *233-234*, 351. (c) Park, J.; Feng, D.; Yuan, S.; Zhou, H. C. *Angew. Chem., Int. Ed.* **2015**, *54*, 430.

(5) (a) Wang, K.; Feng, D.; Liu, T.-F.; Su, J.; Yuan, S.; Chen, Y.-P.; Bosch, M.; Zou, X.; Zhou, H. C. *J. Am. Chem. Soc.* **2014**, *136*, 13983.

(6) Férey, G.; Mellot-Draznieks, C.; Serre, C.; Millange, F.; Dutour, J.; Surblé, S.; Margiolaki, I. *Science* **2005**, *309*, 2040.

(7) (a) De Groot, F. *Chem. Rev.* **2001**, *101*, 1779. (b) Beyzavi, M. H.; Klet, R. C.; Tussupbayev, S.; Borycz, J.; Vermeulen, N. A.; Cramer, C. J.; Stoddart, J. F.; Hupp, J. T.; Farha, O. K. *J. Am. Chem. Soc.* **2015**, *137*, 13624.

(8) Feng, D.; Wang, K.; Wei, Z.; Chen, Y.-P.; Simon, C.; Arvapally, R. K.; Yuan, D.; Omary, M. A.; Haranczyk, M.; Smit, B.; Zhou, H. C. *Nat. Commun.* **2014**, *5*, 5723.

(9) Chou, S. Y.; Krauss, P. R.; Renstrom, P. J. *Science* **1996**, *272*, 85.

(10) (a) Dorenbos, P. *Phys. Rev. B: Condens. Matter Mater. Phys.* **2000**, *62*, 15640. (b) Wang, D. H.; Wang, L.; Xu, A. W. *Nanoscale* **2012**, *4*, 2046. (c) Parr, R. G.; Pearson, R. G. *J. Am. Chem. Soc.* **1983**, *105*, 7512.

(11) Shannon, R. D. *Acta Crystallogr., Sect. A: Cryst. Phys., Diffr., Theor. Gen. Crystallogr.* **1976**, *32*, 751.

(12) Pauling, L. *J. Am. Chem. Soc.* **1932**, *54*, 3570.

(13) (a) Hayyan, M.; Hashim, M. A.; AlNashef, I. M. *Chem. Rev.* **2016**, *116*, 3029. (b) Hirakawa, T.; Nosaka, Y. *Langmuir* **2002**, *18*, 3247. (c) Saito, H.; Nosaka, Y. *J. Phys. Chem. C* **2014**, *118*, 15656. (d) Xu, H. Q.; Hu, J.; Wang, D.; Li, Z.; Zhang, Q.; Luo, Y.; Jiang, H. L. *J. Am. Chem. Soc.* **2015**, *137*, 13440.

(14) (a) Odoh, S. O.; Cramer, C. J.; Truhlar, D. G.; Gagliardi, L. *Chem. Rev.* **2015**, *115*, 6051. (b) Tada, H.; Jin, Q.; Nishijima, H.; Yamamoto, H.; Fujishima, M.; Okuoka, S. I.; Kobayashi, H. *Angew. Chem., Int. Ed.* **2011**, *50*, 3501. (c) Koppenol, W. H. *Nature* **1976**, *262*, 420.




DOI: 10.1021/jacs.6b08724
J. Am. Chem. Soc. 2016, 138, 13822−13825